ESRF	**Experiment title:** **Phase diagram and local structure of $Gd_2(Zr_{1-x}Ti_x)_2O_7$ and $(Gd_{1-y}Nd_y)_2(Zr_{1-z}Ce_z)_2O_7$ pyrochlore matrices for nuclear waste disposal**	**Experiment number**: **CH-5900**
Beamline: ID22	**Date of experiment**: from: 13/04/2021 to: 17/04/2021	**Date of report**: 15/09/2021
Shifts: 12	**Local contact(s)**: CONFALONIERI Giorgia	*Received at ESRF:*

Names and affiliations of applicants (* indicates experimentalists):

Armando di Biase, Marco Scavini, Carlo Castellano, Francesco Demartin
Università degli Studi di Milano, Dip. di Chimica, Milano, Italy

Report

Introduction

Owing to its radiation resistance, $Gd_2Zr_2O_7$ is a potential matrix for incorporating radionuclides. In experiments simulating the α-decay of embedded radionuclides with ion beam irradiation, it has been demonstrated that the susceptibility to radiation-induced amorphization in the system $Gd_2(Zr_{1-x}Ti_x)_2O_7$ steadily decreases with increasing Zr-content. When irradiated, the structure of Zr-rich compounds dissipates the radiation energy undergoing a phase transition from the pyrochlore to the defect fluorite structure[1]. Fluorite is a highly symmetric structure, (MO_2, space group $Fm\bar{3}m$, Z=4) with one cationic (Wickoff letter *4a*) and one anionic (*8c*) site. Pyrochlore is a fluorite-related superstructure (s.g. $Fd\bar{3}m$, Z=8), which is generally adopted by oxides with formula $A_2B_2O_7$ The A^{3+} and B^{4+} cations are distributed over two crystallographically independent sites with 8-fold (*16d*) and 6-fold (*16c*) coordination respectively, while the oxygen site splits in two occupied tetrahedral interstices (*8b* and *48f*) and an additional empty one (*8b*). The disordering process invoked for $Gd_2Zr_2O_7$ involves the swapping of the cations and the randomization of the anions and the vacancies. Moreover, while in the fluorite all the atomic coordinates are fixed, the pyrochlore structure has one variable positional parameter, which is the *48f*-oxygen x parameter[2]. It is worth citing also weberite, an additional anion-deficient fluorite superstructure with stoichiometry $A_2B_2O_7$, (s.g. $C222_1$, Z=4). Following Ref.[3] for the case of $Ho_2Zr_2O_7$, A and B cations occupy eight-coordinated and six-coordinated *4b* sites respectively, while the seven coordinated *8c* site is shared by both cations. At the same time, oxygen ions occupy three sites with multiplicity 4 (all *4a*) and two with multiplicity 8 (all *8c*), leaving an empty site of multiplicity 4 in respect of fluorite structure. Weberite structure allows several cationic and anionic degrees of freedom, which makes it a model structure to reproduce the cation swapping of the pyrochlore structure induced by radiation damage.

The structures of the $Gd_2(Zr_{1-x}Ti_x)_2O_7$ solid solution and selected $(Gd_{1-y}Nd_y)_2(Zr_{1-z}Ce_z)_2O_7$ compositions were investigated by means of high-resolution powder diffraction measurements coupled with the real-space Pair Distribution Function (PDF) analysis. The data analysis enabled us to describe the structure of these candidate waste forms at different length scales in terms of the phase relations between the fluorite and its superstructures.

Samples & Data collection strategy

Pyrochlore samples of composition: $Gd_2(Zr_{1-x}Ti_x)_2O_7$ (x=0, 0.15, 0.25, 0.50, 0.75, 0.85, 1) and $(Gd_{1-y}Nd_y)_2(Zr_{1-z}Ce_z)_2O_7$ with all the possible combinations of y, z = 0.00, 0.25 and 0.50 were prepared by solid-state reaction, firing the pelletized mixture of starting oxide at 1500 °C for 24h for several times (5-7) with intermediate grindings and re-pelletizing until a homogeneous material was obtained.

XRPD patterns were collected at the ID22 beamline on powdered samples at RT and 90 K using the high-resolution set-up of ID22 (λ = 0.35417647 Å) for Rietveld refinements and the 2-D detector (λ = 0.17712028 Å) for PDF analysis

Results:

We will present here and discuss only results from data collected at 90 K since the RT ones show similar trends. Moreover, we will skip the data on double doped samples because the analysis of their complex behaviour at the local scale is still in progress.

In Figure 1 are shown as examples two Rietveld Refinements on patterns collected on $Gd_2Zr_2O_7$ (A) and Gd_2ZrCeO_7 (E) samples. As to the $Gd_2(Ti_{1-x}Zr_x)_2O_7$ solid solution (GZT SS), all the samples take the pyrochlore structure. Raising the Zr concentration also the cell constant (Fig.1B), the xO1 coordinate (Fig.1C) and the average atomic mean square displacement parameter Ueq (Fig.1D) increased monotonically. The first trend is expected, due to the different ionic radii of Ti^{4+}(VI) and Zr^{4+}(VI). The second one points to the transition toward the defect fluorite structure, while the third one is a clear indication of progressive structural disordering: roughly speaking, U_{eq} values are the sum of thermal vibration and static disorder contribution. Since all the patterns are collected at the same *T* value, changes in U_{eq} are mainly due to the latter contribution. The same parameters are displayed in Fig.1(F-H) for the $(Gd_{1-x}Nd_x)_2Zr_2O_7$ and $Gd_2(Zr_{1-y}Ce_y)_2O_7$ systems. We skip double doped samples here for sake of clarity. $(Gd_{1-x}Nd_x)_2Zr_2O_7$ samples display pyrochlore structure while $Gd_2(Zr_{1-y}Ce_y)_2O_7$ ones take a defective fluorite one. For this reason xO1 is fixed to 0.375 value in the latter case. U_{eq} values follow two different trends on increasing x or y. Ce doping boosts disorder while Nd doping determines exactly the opposite effect. We stress the importance of this evidence: since Ce and Nd doping should mime the crystal evolution of Am and Pu doped $Gd_2Zr_2O_7$, the structure ordering effect of neodimium has to be considered to tune suitably the Am and Pu concentration in order to dispose nuclear wastes in robust crystalline phases.

Obviously U_{eq} analysis supplies only qualitative trends. Local probes such as EXAFS and PDF are fundamental to get an accurate picture of the structural evolution at different scale lengths.

The PDF/G(r) functions of selected samples are shown together in Figure 2. The local structure of $Gd_2Ti_2O_7$ perfectly matches the average one as testified by the good fit and fit residuals (Rw=0.070) using the pyrochlore model. See Fig.2A. As shown in Figs.2B-C the fit quality decreases on raising the xZr to 0.5 thus confirming that Zr doping induces disorder. A much better fit of $Gd_2Zr_2O_7$ PDF derives by the application of the weberite model (see Fig.2D): some cation positions swapping and oxygen disorder is induced by Zr doping.

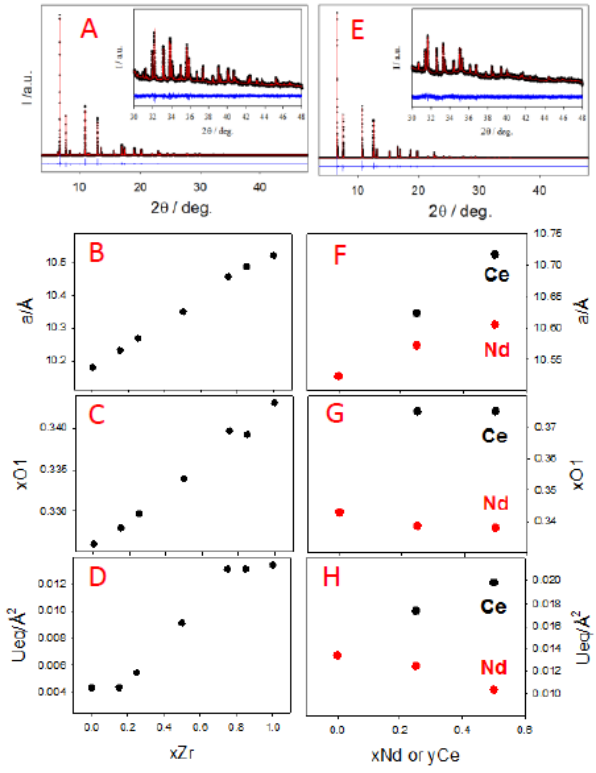

Figure 1. Rietveld refinements of XRPD patterns collected at 90K on on $Gd_2Zr_2O_7$ (**A**) and Gd_2ZrCeO_7 (**E**) samples. Refined parameters on the $Gd_2(Ti_{1-x}Zr_x)_2O_7$ (**B-D**) and on $(Gd_{1-x}Nd_x)_2Zr_2O_7$ and $Gd_2(Zr_{1-y}Ce_y)_2O_7$ systems (**F-H**).

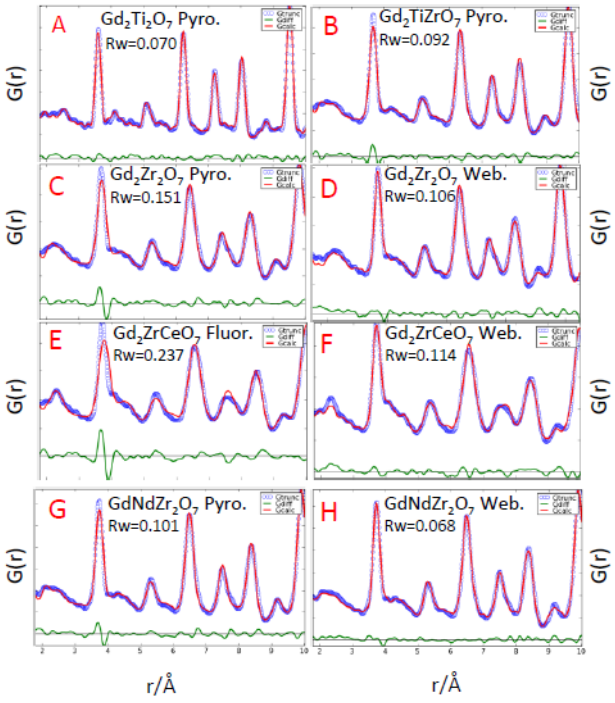

Figure 2. Low *r* portions of selected G(r) functions collected at 90 K together to fits using either the structural models from the Rietveld analysis (panels A-C, E, G) or the Weberite structure (panels D, F, H). See Text for details. Pyro., Fluor. And Web., refer to pyrochlore, fluorite and weberite structures, respectively.

The structure of Gd_2ZrCeO_7 is fluorite on average. However, the fit of G(r) with this model brings to an awful fit. For this compound likewise, some improvement in the fit is achieved applying the weberite model. However, some structural mismatches appear even at the local scale. Disorder in the $Gd_2(Zr_{1-y}Ce_y)_2O_7$ system is even more complex than in pure $Gd_2Zr_2O_7$. This is not unexpected. In fact, it is known that the endmember at the opposite side of this solid solution

($Gd_2Ce_2O_7$) i) is C-type without any Ce/Gd cation ordering on average and ii) is formed by coexisting CeO_2 and Gd_2O_3 droplets-like domains at the local scale[4,5]. Thus, the $Gd_2(Zr_{1-y}Ce_y)_2O_7$ system displays a complex structural behaviour both at the local and at the average scales that deserves to be investigated in further detail extending the number of investigated compositions in the whole y range.

Finally, Fig.2G reports the exp. G(r) of $GdNdZr_2O_7$ along with its fit using pyrochlore model. The residuals suggest that some pyrochlore ordering is recovered in respect to the x=0 end member $Gd_2Zr_2O_7$, which is in line with the reciprocal space analysis but unexpected since solid solutions generally exhibit larger disorder degree than the pure compounds. The weberite model allows to interpret the residual disorder of $GdNdZr_2O_7$ (see Fig.2H).

It should be noted that a good fit quality is recovered in all cases, fitting the G(r) function at larger *r* ranges probing that the weberite-like domains have coherence lengths of the order of few nanometers. Then, the long range structure is recovered.

Summarising, passing from $Gd_2Ti_2O_7$ to $Gd_2Zr_2O_7$, disorder is raised and consists of nanodomains dominated by cations and oxygens disorder, which resembles that of the weberite structure. Focusing on $Gd_2Zr_2O_7$, which is a promising candidate for nuclear waste disposal, Ce or Nd doping have opposite effects on disorder. While Ce doping boosts disorder in a complex way, varying the Zr/Ce amount, Nd doping has the opposite effect. It reduces disorder, at least up to x=0.5.

Future developments

Both single doped and the double doped systems deserve to be more deeply investigated, completing the analysis of their phase diagrams at different length scales for several reasons: a) they are interesting *per se* due to their complex behaviour varying the compositional coordinates; b) radiation damage of $Gd_2Zr_2O_7$ brings to progressive transformation of the average structure from the pyrochlore to the fluorite structure; thus moving along the y coordinate in $Gd_2(Zr_{1-y}Ce_y)_2O_7$ should mime the same effect; c) since Nd doping of $Gd_2Zr_2O_7$ contributes to reduce disorder, a full understanding of its role in single and double doped samples should allow to plan Am and/or Pu doped $Gd_2Zr_2O_7$ samples for nuclear waste disposal with enhanced resistance to radiation damage.

The combined use of HR-XRPD and PDF analysis has proved to be an effective way to address these problems and accurately maps the structures at different length scales. Also EXAFS measurements would play an important and complementary role in mapping the cations environments. In fact, in these very symmetric multi-element systems, coordination shells (1^{st}-M-O, 2^{nd}-M-M…) of different cations drop at similar interatomic distances. EXAFS would complete the PDF analysis supplying unique element-sensitive information on cations environments at the very local scale.

References

[1] S.X. Wang et *al.*, J. Mater. Res. 14 (1999) 4470–4473.

[2] M.A. Subramanian et *al.*, Prog. Solid State Chem. 15 (1983) 55–143.

[3] D.L. Drey et *al.*, RSC Adv. 10 (2020) 34632–34650.

[4] M. Scavini et *al.*, Chem. Mater. 24 (2012) 1338–1345.

[5] M. Scavini et *al.*, IUCrJ. 2 (2015) 511–522.